Uniform Semiglobal Exponential Stability of Integral Line-of-Sight Guidance Laws[*]

Martin S. Wiig [*,†] **Kristin Y. Pettersen** [*,†]
Thomas R. Krogstad [†]

[*] *Centre for Autonomous Marine Operations and Systems (AMOS),*
Department of Engineering Cybernetics, Norwegian University of
Science and Technology, 7491 Trondheim, Norway.
E-mail: {Martin.Wiig, Kristin.Y.Pettersen}@itk.ntnu.no
[†] *Norwegian Defence Research Establishment (FFI), P.O. Box 25,*
N-2027 Kjeller, Norway.
E-mail: Thomas-Robekk.Krogstad@ffi.no

Abstract: This paper proves that an integral line-of-sight guidance law for path following control of underactuated marine vessels provides uniform semiglobal exponential stability. The stability result is stronger than what has been proved in previous literature, with stronger convergence properties and more robustness. The analysis is based on the 3-dimensional maneuvering control model of marine vessels, which describes both surface vessels and underwater vehicles moving in a horizontal plane. Both the kinematics and dynamics of the system is taken into account, as well as disturbances from constant and irrotational ocean currents. Simulation results are presented to validate the theoretical analysis.

Keywords: path following, guidance systems, LOS guidance, underactuated vessel, disturbance compensation, exponentially stable, cascade control

1. INTRODUCTION

Marine vessels rely on guidance systems to achieve desired control scenarios such as path following, path tracking and path maneuvering. Descriptions of these motion control scenarios are given in Encarnação and Pascoal (2001), Breivik and Fossen (2009) and Fossen (2011). In particular, operations such as inspection of submarine pipelines, seabed mapping and environmental monitoring require precise path following. Vehicles used in such operations are often underactuated as they are equipped with fixed stern propellers and steering rudders. Guidance laws made for underactuated vehicles are thus of particular importance.

The line-of-sight (LOS) path following principle, used in Healey and Lienard (1993), Pettersen and Lefeber (2001), Fossen et al. (2003), Breivik and Fossen (2004) and Fredriksen and Pettersen (2006), mimics the way an experienced helmsman steers a ship by aiming towards a point that lies on the path ahead of the vessel. Pettersen and Lefeber (2001) proved uniform global κ-exponential stability (defined in Sørdalen and Egeland (1995) as global asymptotic stability (UGAS) and uniform local exponential stability (ULES)) of the LOS guidance law in connection with a simplified vehicle model in 3 degrees of freedom (3-DOF). The results were extended to include a more complete 3-DOF vehicle model in Børhaug and Pettersen (2005) and Fredriksen and Pettersen (2006). Even more robust stability properties was shown in Fossen and

Pettersen (2014), where uniform semiglobal exponential stability (USGES) of the LOS guidance was proved.

To compensate for drift caused by environmental disturbances such as current, Børhaug et al. (2008) added integral action to the LOS guidance law. The resulting integral line-of-sight (ILOS) guidance law was proved to be globally stable. This result was extended to global κ-exponential stability in Caharija et al. (2012a), Caharija et al. (2012b) and Caharija et al. (2014).

The above references on ILOS guidance consider kinematic ocean current as the only disturbance affecting motion. In Caharija et al. (2013), effects of disturbances from winds, waves and currents on the kinetic level are investigated, while the kinematic disturbances are ignored. Global κ-exponential stability of the ILOS guidance law in closed loop with the kinematic model is proved. Caharija et al. (2015) combines the kinematic and kinetic disturbance models and proves global κ-exponential stability of the ILOS guidance law in combination with a vessel model containing kinematics and dynamics. Caharija et al. (2015) also examines the stability properties of a 3 dimensional ILOS guidance law for an underwater vehicle modeled in 5-DOF, again proving global κ-exponential stability of the system.

Fossen et al. (2014) modifies the integral term used in Børhaug et al. (2008) to achieve integral action using adaptive sideslip estimation, and is able to prove USGES for a closed loop kinematic model of an underactuated marine vehicle following Dubins paths (Dubins (1957)). Lekkas and Fossen (2014) proves that a similar system

is globally κ-exponentially stable when following paths parametrized as monotone cubic Hermite splines.

This paper considers a 3-DOF vessel model including the kinematics and dynamics of the vessel, as well as kinematic disturbances from constant and irrotational ocean currents. The main contribution is an extension of the result of Caharija et al. (2012a) and Caharija et al. (2014), using the methods of Fossen and Pettersen (2014) to prove that an underactuated marine vessel controlled by the ILOS guidance law achieves the stronger stability results of USGES and UGAS.

USGES provides stronger convergence and robustness properties than the previous results of κ-exponential stability. In particular, it follows from (Khalil, 2002, Lemma 9.2) that the USGES property implies that a sufficiently large region of attraction in which there is exponential convergence can always be chosen. Hence, the solution of the perturbed system will be uniformly bounded regardless of the size of the perturbation. This is a stronger robustness property than for κ-exponential stability, which according to (Khalil, 2002, Lemma 9.3) requires the perturbation to be small to ensure a uniformly bounded solution. Note that UGES cannot be achieved with ILOS or LOS guidance laws due to saturation introduced through trigonometric functions in the kinematic representation.

This paper is organized as follows. Section 2 gives a description of the vehicle model in 3-DOF, and states the control objective. Section 3 describes the ILOS guidance law and the surge and speed controllers that are analyzed in this paper. A stability analysis of the closed-loop kinematic system is presented in Section 4, while the stability of the complete closed-loop kinematic and dynamic system is analyzed in Section 5. The analyzes show both systems to be USGES, which is the main result of this paper. Simulations that demonstrate the exponential stability of the system are shown in Section 6.

2. SYSTEM DESCRIPTION

2.1 System Model

The vehicle is modeled in 3-DOF with $\boldsymbol{p} \triangleq [x, y, \psi]^T$ containing position and orientation in the inertial frame i. The body-fixed velocity of the vessel is represented by $\boldsymbol{\nu} \triangleq [u, v, r]^T$, where u is the surge speed, v is the sway speed and r is the yaw rate.

The following assumption is made on the ocean current:

Assumption 1. The ocean current $\boldsymbol{v}_c \triangleq [V_x, V_y, 0]^T$ in i is assumed to be constant, irrotational and bounded. Hence, there exists a constant $V_{\max} \geq 0$ such that $V_{\max} \geq \sqrt{V_x^2 + V_y^2}$.

The current velocity in the body frame b is $\boldsymbol{\nu}_c = \boldsymbol{R}^T(\psi)\boldsymbol{v}_c = [u_c, v_c, 0]^T$, where $\boldsymbol{R}(\psi)$ is the rotation matrix from b to i given in by

$$\boldsymbol{R}(\psi) \triangleq \begin{bmatrix} \cos(\psi) & -\sin(\psi) & 0 \\ \sin(\psi) & \cos(\psi) & 0 \\ 0 & 0 & 1 \end{bmatrix}. \tag{1}$$

From Assumption 1 it follows that $\dot{\boldsymbol{v}}_c = \boldsymbol{0}$ and $\dot{\boldsymbol{\nu}}_c = [rv_c, -ru_c, 0]^T$.

In the presence of constant and irrotational current, the vessel model can be represented in terms of the relative velocities as described in Fossen (2011). The body-fixed relative velocity is given by $\boldsymbol{\nu}_r \triangleq \boldsymbol{\nu} - \boldsymbol{\nu}_c = [u_r, v_r, r]^T$, where u_r is the relative surge speed and v_r is the relative sway speed. The vehicle can then be represented by the 3-DOF model

$$\dot{\boldsymbol{p}} = \boldsymbol{R}(\psi)\boldsymbol{\nu}_r + \boldsymbol{\nu}_c, \tag{2a}$$
$$\boldsymbol{M}\dot{\boldsymbol{\nu}}_r + \boldsymbol{C}(\boldsymbol{\nu}_r)\boldsymbol{\nu}_r + \boldsymbol{D}\boldsymbol{\nu}_r = \boldsymbol{B}\boldsymbol{f}, \tag{2b}$$

where $\boldsymbol{M} = \boldsymbol{M}^T > 0$ is the mass and inertia matrix including hydrodynamic added mass, $\boldsymbol{C}$ is the Coriolis and centripetal matrix, $\boldsymbol{D} > 0$ is the linear hydrodynamic damping matrix and $\boldsymbol{B} \in \mathbb{R}^{3 \times 2}$ is the actuator configuration matrix. $\boldsymbol{f} \triangleq [T_u, T_r]^T$ is the control input vector with surge thrust T_u and the rudder angle T_r.

Nonlinear damping terms such as nonlinear cross flow drag effects are not considered. However, the passive nature such damping forces should enhance the directional stability of the ship, as noted in Caharija et al. (2012a).

$\boldsymbol{C}$ is obtained from $\boldsymbol{M}$ as described in Fossen (2011), while the other system matrices can be expressed as:

$$\boldsymbol{M} \triangleq \begin{bmatrix} m_{11} & 0 & 0 \\ 0 & m_{22} & m_{23} \\ 0 & m_{23} & m_{33} \end{bmatrix}, \tag{3}$$

$$\boldsymbol{D} \triangleq \begin{bmatrix} d_{11} & 0 & 0 \\ 0 & d_{22} & d_{23} \\ 0 & d_{32} & d_{33} \end{bmatrix}, \boldsymbol{B} \triangleq \begin{bmatrix} b_{11} & 0 \\ 0 & b_{22} \\ 0 & b_{33} \end{bmatrix}. \tag{4}$$

The structure of the system matrices is obtained by assuming that the vehicle is port-starboard symmetric, and that the origin of b is located in a point $(x_g^*, 0)$ along the centerline of the vessel. x_g^* lies on the pivot point of the ship, removing the control input τ_r from the sway dynamics. This means that $\boldsymbol{M}^{-1}\boldsymbol{B}\boldsymbol{f} = [\tau_u, 0, \tau_r]^T$, where τ_u is the control force in surge and τ_r is the control moment in yaw. If b is not originally located in x_g^* the coordinate system can be translated to the pivot point using a coordinate transform as described in Fossen (2011).

2.2 System Model in Component Form

The 3-DOF model in (2) can be represented in component form:

$$\dot{x} = u_r \cos(\psi) - v_r \sin(\psi) + V_x, \tag{5a}$$
$$\dot{y} = u_r \sin(\psi) + v_r \cos(\psi) + V_y, \tag{5b}$$
$$\dot{\psi} = r, \tag{5c}$$
$$\dot{u}_r = F_{u_r}(v_r, r) - \frac{d_{11}}{m_{11}}u_r + \tau_u, \tag{5d}$$
$$\dot{v}_r = X(u_r)r + Y(u_r)v_r, \tag{5e}$$
$$\dot{r} = F_r(u_r, v_r, r) + \tau_r. \tag{5f}$$

$F_{u_r}(v_r, r)$, $X(u_r)$, $Y(u_r)$ and $F_r(u_r, v_r, r)$ are defined in Appendix A. The following bound is assumed on $Y(u_r)$:

Assumption 2. The function $Y(u_r)$ satisfies

$$Y(u_r) \leq -Y_{\min} < 0, \quad \forall u_r \in [-V_{\max}, U_{rd}]. \tag{6}$$

This is justified by noticing that $Y(u_r) > 0$ implies that the system is undamped or nominally unstable in sway, which is not the case for commercial vessels by design.

2.3 Control objective

The objective of the control system is to make the vehicle modeled by (2) converge to and follow a straight-line path. This objective should be met in the presence of unknown, constant and irrotational current while keeping a constant relative surge speed $U_{rd} > 0$. To simplify the analysis, without any loss of generality, the inertial reference frame i is placed such that its x-axis is aligned with the desired path $\mathcal{P}$, $\mathcal{P} \triangleq \{(x, y) \in \mathbb{R}^2 : y = 0\}$. The objectives of the control system are formalized as

$$\lim_{t \to \infty} y(t) = 0, \tag{7a}$$

$$\lim_{t \to \infty} \psi(t) = \psi_{ss}, \quad \psi_{ss} \in \left(-\frac{\pi}{2}, \frac{\pi}{2}\right), \tag{7b}$$

$$\lim_{t \to \infty} u_r(t) = U_{rd}, \tag{7c}$$

where ψ_{ss} is a constant yaw angle required to keep the underactuated vessel at the path in the presence of current. Note that, even though the vessel will sideslip along the path, the drift angle with respect to the water flow will converge to zero due to port-starboard symmetry. The following assumption ensures that the vessel is able to follow the path for any direction of the ocean current:

Assumption 3. The propulsion system is capable of achieving a U_{rd} such that $U_{rd} > V_{\max}$.

3. CONTROL SYSTEM

This section presents a control system for the path following problem presented in Section 2.3.

3.1 The ILOS guidance law

The desired heading ψ_d is given by the ILOS guidance law introduced in Børhaug et al. (2008):

$$\psi_d \triangleq -\tan^{-1}\left(\frac{y + \sigma y_{\text{int}}}{\Delta}\right), \quad \Delta > 0, \quad \sigma > 0, \tag{8a}$$

$$\dot{y}_{\text{int}} \triangleq \frac{\Delta y}{(y + \sigma y_{\text{int}})^2 + \Delta^2}. \tag{8b}$$

The look-ahead distance Δ and the integral gain σ are constant design parameters. The integral effect creates a nonzero desired heading even when the cross-track error is zero. Without this effect, any ocean current acting in the transversal direction of the desired path would push the vessel away from the path and thus create a steady state error. By design, the integral term growth rate (8b) will decrease for large cross-track errors y, reducing the risk of wind-up effects.

3.2 Surge and yaw controllers

Surge and yaw are controlled using the feedback linearizing controllers described in Caharija et al. (2012a):

$$\tau_u = -F_{u_r}(v_r, r) + \frac{d_{11}}{m_{11}} U_{rd} + \dot{u}_{rd} - k_{u_r}(u_r - U_{rd}), \tag{9}$$

$$\tau_r = -F_r(u_r, v_r, r) + \ddot{\psi} - k_\psi(\psi - \psi_d) - k_r(\dot{\psi} - \dot{\psi}_d), \tag{10}$$

where k_{u_r}, k_ψ and k_r are constant, positive gains.

4. CLOSED-LOOP KINEMATIC STABILITY

This section analyzes the stability properties of the closed-loop kinematic system by assuming zero sway speed v_r and perfectly controlled surge $u_r = U_{rd}$ and heading $\psi = \psi_d$. Substituting (8a) into (5b) then gives the following expression for the y kinematics:

$$\dot{y}_{\text{int}} = \frac{\Delta y}{(y + \sigma y_{\text{int}})^2 + \Delta^2}, \tag{11a}$$

$$\dot{y} = -U_{rd} \frac{y + \sigma y_{\text{int}}}{\sqrt{(y + \sigma y_{\text{int}})^2 + \Delta^2}} + V_y. \tag{11b}$$

The equilibrium point of (11) is given by

$$y_{\text{int}}^{\text{eq}} = \frac{\Delta}{\sigma} \frac{V_y}{\sqrt{U_{rd}^2 - V_y^2}}, \quad y^{\text{eq}} = 0. \tag{12}$$

Note that the saturation introduced by the sinusoidal function of the y dynamics in (5b) makes the system gain in (11) decrease with the magnitude of the cross-track error. Hence, GES cannot be achieved.

Theorem 1. If Assumptions 1 and 3 hold and the gain σ satisfies

$$0 < \sigma < U_{rd} - V_{max}, \tag{13}$$

then the ILOS guidance law (8) applied to the cross-track error dynamics (11) renders the equilibrium point (12) USGES.

Proof. The proof follows along the lines of Caharija et al. (2012a) and Caharija et al. (2014), while also making use of the comparison lemma (Khalil, 2002, Lemma 3.4) along the lines of the analysis in Fossen and Pettersen (2014).

A change of variables is introduced to obtain a system with the equilibrium point at the origin:

$$e_1 \triangleq y_{\text{int}} - y_{\text{int}}^{\text{eq}}, \quad e_2 \triangleq y + \sigma e_1. \tag{14}$$

The dynamics of the shifted system are:

$$\dot{e}_1 = -\frac{\Delta \sigma e_1}{h(e_2)} + \frac{\Delta e_2}{h(e_2)}, \tag{15}$$

$$\dot{e}_2 = -\frac{\Delta \sigma^2 e_1}{h(e_2)} + V_y f(e_2)$$
$$- \left[U_{rd}\sqrt{h(e_2)} - \sigma\Delta\right] \frac{e_2}{h(e_2)}, \tag{16}$$

where $h(e_2)$ is defined as

$$h(e_2) \triangleq (e_2 + \sigma y_{\text{int}}^{\text{eq}})^2 + \Delta^2, \tag{17}$$

and $f(e_2)$ is defined as

$$f(e_2) \triangleq 1 - \frac{\sqrt{(\sigma y_{\text{int}}^{\text{eq}})^2 + \Delta^2}}{\sqrt{h(e_2)}}. \tag{18}$$

The following bound holds for $f(e_2)$:

$$|f(e_2)| \leq \frac{|e_2|}{\sqrt{h(e_2)}} \tag{19}$$

Consider the Lyapunov function candidate

$$V = \frac{\sigma^2}{2} e_1^2 + \frac{1}{2} e_2^2 = \frac{1}{2} \boldsymbol{e}^\top \boldsymbol{P} \boldsymbol{e}, \tag{20}$$

where $\boldsymbol{e} \triangleq [e_1, e_2]^\top$ and $\boldsymbol{P} \triangleq \text{diag}\{\sigma^2, 1\} > 0$. The time-derivative of V is

$$\dot{V} = - \left[U_{rd}\sqrt{h(e_2)} - \sigma\Delta \right] \frac{e_2^2}{h(e_2)}$$
$$- \frac{\Delta\sigma^3 e_1^2}{h(e_2)} + V_y f(e_2), \tag{21}$$

which can be shown to satisfy

$$\dot{V} \le -\frac{1}{h(e_2)} \boldsymbol{e}^\top \boldsymbol{Q} \boldsymbol{e}, \tag{22}$$

where Q is defined as

$$\boldsymbol{Q} \triangleq \mathrm{diag}\{\sigma^3, \Delta(U_{rd} - V_{\max} - \sigma)\}. \tag{23}$$

Under the assumption that σ satisfies (13), $\boldsymbol{Q} > 0$ and hence $\dot{V} \le 0$. By (Khalil, 2002, Theorem 4.8), this implies that the equilibrium $\boldsymbol{e} = \boldsymbol{0}$ is uniformly stable.

The term $\sigma y_{\mathrm{int}}^{\mathrm{eq}}$ in (17) can be bounded using (12) and Assumption 1 to

$$\sigma y_{\mathrm{int}}^{\mathrm{eq}} = \frac{\Delta V_y}{\sqrt{U_{rd}^2 - V_y^2}} \le \frac{\Delta V_{\max}}{\sqrt{U_{rd}^2 - V_{\max}^2}} := \kappa. \tag{24}$$

Hence

$$\dot{V} \le -\frac{1}{(e_2 + \kappa)^2 + \Delta^2} \boldsymbol{e}^\top \boldsymbol{Q} \boldsymbol{e}. \tag{25}$$

Furthermore, for each $r > 0$ and $|e_2| \le r$ we have

$$\frac{1}{(e_2 + \kappa)^2 + \Delta^2} \ge \frac{1}{(r + \kappa)^2 + \Delta^2} := c(r). \tag{26}$$

Consequently,

$$\dot{V} \le -c(r)\boldsymbol{e}^\top \boldsymbol{Q} \boldsymbol{e} \le -2c(r)\frac{q_{\min}}{p_{\max}} V, \ \forall \|\boldsymbol{e}(t)\| \le r, \tag{27}$$

where $p_{\max} = \max\{\sigma^2, 1\}$ and $q_{\min} = \min\{\sigma^3, \Delta(U_{rd} - V_{\max} - \sigma)\}$.

The inequality in (27) is valid for all trajectories generated by the initial conditions $\boldsymbol{e}(t_0)$ since the system is uniformly stable. The comparison lemma can be invoked by noticing that the linear system $\dot{z} = -2(q_{\min}/p_{\max})c(r)z$ has the solution $z(t) = e^{-2(q_{\min}/p_{\max})c(r)(t-t_0)}z(t_0)$. This implies that $v(t) \le e^{-2(q_{\min}/p_{\max})c(r)(t-t_0)}v(t_0)$ for $v(t) = V(t, \boldsymbol{e}(t))$. Hence,

$$\|\boldsymbol{e}(t)\| \le \sqrt{\frac{p_{\max}}{p_{\min}}} e^{-\frac{q_{\min}}{p_{\max}}c(r)(t-t_0)} \|\boldsymbol{e}(t_0)\|, \tag{28}$$

where $p_{\min} \triangleq \min\{\sigma^2, 1\}$. This holds for all $t \ge t_0, \|\boldsymbol{e}(t)\| \le r$ and any $r > 0$, and it shows the equilibrium point $\boldsymbol{e} = \boldsymbol{0}$ to be USGES (Loria and Panteley, 2004, Definition 2.7).

5. STABILITY OF THE CLOSED-LOOP KINEMATICS AND DYNAMICS

This section analyzes the stability properties of the complete vessel kinematics and dynamics with the ILOS guidance law (8) in a cascaded configuration with the surge and yaw controllers (9)-(10), proving USGES of the equilibrium point of the resulting closed-loop system. In the following, the notation $X^{U_{rd}} = X(U_{rd})$ and $Y^{U_{rd}} = Y(U_{rd})$ is used for brevity.

5.1 Cascaded system description

The error signals in surge, sway and yaw are collected in $\boldsymbol{\zeta} \triangleq [\tilde{u}_r, \tilde{\psi}, \dot{\tilde{\psi}}]^T$, where $\tilde{u}_r \triangleq u_r - U_{rd}$, $\tilde{\psi} = \psi - \psi_d$ and

$\dot{\tilde{\psi}} \triangleq r - \dot{\psi}_d$. The dynamics of $\boldsymbol{\zeta}$ are obtained by combining the system equations (5c), (5d) and (5f) with the control laws in surge (9) and yaw (10):

$$\dot{\boldsymbol{\zeta}} = \begin{bmatrix} -k_{u_r} - \dfrac{d_{11}}{m_{11}} & 0 & 0 \\ 0 & 0 & 1 \\ 0 & -k_\psi & -k_r \end{bmatrix} \boldsymbol{\zeta} \triangleq \boldsymbol{\Sigma}\boldsymbol{\zeta}. \tag{29}$$

The $y - v_r$ subsystem is then obtained from (5b), (5e) and (8b):

$$\dot{y}_{\mathrm{int}} = \frac{\Delta y}{(y + \sigma y_{\mathrm{int}})^2 + \Delta^2}, \tag{30a}$$
$$\dot{y} = (\tilde{u}_r + U_{rd})\sin(\tilde{\psi} + \psi_d) + v_r\cos(\tilde{\psi} + \psi_d) + V_y, \tag{30b}$$
$$\dot{v}_r = X(\tilde{u}_r + U_{rd})(\dot{\tilde{\psi}} + \dot{\psi}_d) + Y(\tilde{u}_r + U_{rd})v_r. \tag{30c}$$

The equilibrium point of (30) on the manifold $\boldsymbol{\zeta} = \boldsymbol{0}$ is given by

$$y_{\mathrm{int}}^{\mathrm{eq}} = \frac{\Delta}{\sigma}\frac{V_y}{\sqrt{U_{rd}^2 - V_y^2}}, \quad y^{\mathrm{eq}} = 0, \quad v_r^{\mathrm{eq}} = 0. \tag{31}$$

A change of variables is introduced to obtain a system with the equilibrium point at the origin:

$$e_1 \triangleq y_{\mathrm{int}} - y_{\mathrm{int}}^{\mathrm{eq}}, \ e_2 \triangleq y + \sigma e_1, \ e_3 \triangleq v_r. \tag{32}$$

After factorizing with respect to $\boldsymbol{\zeta}$, the interconnected dynamics of (29) and (30) can be expressed in cascade form as

$$\dot{\hat{\boldsymbol{e}}} = \boldsymbol{A}(e_2)\hat{\boldsymbol{e}} + \boldsymbol{B}(e_2) + \boldsymbol{H}(e_2, e_3, \psi_d, \boldsymbol{\zeta})\boldsymbol{\zeta}, \tag{33a}$$
$$\dot{\boldsymbol{\zeta}} = \boldsymbol{\Sigma}\boldsymbol{\zeta}, \tag{33b}$$

where $\hat{\boldsymbol{e}} \triangleq [e_1, e_2, e_3]^T$, $\boldsymbol{A}$ is given in (35) while

$$\boldsymbol{B}(e_2) \triangleq \begin{bmatrix} 0 \\ V_y f(e_2) \\ -\dfrac{\Delta X^{U_{rd}} V_y}{h(e_2)} f(e2) \end{bmatrix}. \tag{34}$$

The interconnection matrix $\boldsymbol{H}$ contains all the terms vanishing at $\boldsymbol{\zeta} = 0$ and is given by

$$\boldsymbol{H}(e_2, e_3, \psi_d, \boldsymbol{\zeta}) \triangleq \begin{bmatrix} 0 & 0 \\ 1 & 0 \\ -\dfrac{\Delta X(\tilde{u}_r + U_{rd})}{h(e_2)} & 1 \end{bmatrix} \begin{bmatrix} \boldsymbol{h}_{e_2}^T \\ \boldsymbol{h}_{e_3}^T \end{bmatrix}, \tag{36}$$

where $\boldsymbol{h}_{e_2}$ and $\boldsymbol{h}_{e_3}$ are given in Appendix A. $f(e_2)$ is as defined (18).

5.2 Stability of the nominal system

The nominal system of the cascade in (33) is

$$\dot{\hat{\boldsymbol{e}}} = \boldsymbol{A}(e_2)\hat{\boldsymbol{e}} + \boldsymbol{B}(e_2). \tag{37}$$

Lemma 2. If Assumptions 1 to 3 hold and the look-ahead distance Δ and the integral gain σ satisfy

$$\Delta > \frac{|X^{U_{rd}}|}{|Y^{U_{rd}}|} \left[\frac{5}{4}\frac{U_{rd} + V_{\max} + \sigma}{U_{rd} - V_{\max} - \sigma} + 1 \right], \tag{38}$$
$$0 < \sigma < U_r - V_{\max}, \tag{39}$$

then the equilibrium point of (37) is USGES.

Proof. The proof follows along the lines of Caharija et al. (2012a) and Caharija et al. (2014), while making use of

$$\boldsymbol{A} \triangleq \begin{bmatrix} -\dfrac{\sigma\Delta}{h(e_2)} & \dfrac{\Delta}{h(e_2)} & 0 \\[2ex] -\dfrac{\sigma^2\Delta}{h(e_2)} & -\dfrac{U_{rd}}{\sqrt{h(e_2)}} + \dfrac{\sigma\Delta}{h(e_2)} & \dfrac{\Delta}{\sqrt{h(e_2)}} \\[2ex] \dfrac{\sigma^2\Delta^2 X^{U_{rd}}}{h(e_2)^2} & \left(\dfrac{U_{rd}\Delta X^{U_{rd}}}{h(e_2)^{3/2}} - \dfrac{\sigma\Delta^2 X^{U_{rd}}}{h(e_2)^2} \right) & \left(Y^{U_r} - \dfrac{\Delta^2 X^{U_{rd}}}{h(e_2)^{3/2}} \right) \end{bmatrix} \tag{35}$$

the comparison lemma (Khalil, 2002, Lemma 3.4) along the lines of the analysis in Fossen and Pettersen (2014).

Consider the Lyapunov function candidate:
$$W \triangleq \tfrac{1}{2}\sigma^2 e_1^2 + \tfrac{1}{2}e_2^2 + \tfrac{1}{2}\mu e_3^2, \quad \mu > 0. \tag{40}$$
Using Assumption 1 and 2, (19) and $ab \leq |a||b|$, the following bound can be found for $\dot{W}$:
$$\dot{W} \leq -L_1(\hat{\boldsymbol{e}}_{13}) - L_2(\hat{\boldsymbol{e}}_{23}), \tag{41}$$
where $\hat{\boldsymbol{e}}_{13} \triangleq [e_1, e_3]^T$ and $\hat{\boldsymbol{e}}_{23} \triangleq [e_2, e_3]^T$. L_1 is defined as
$$L_1 = \frac{1}{h(e_2)} \hat{\boldsymbol{e}}_{13}^T \boldsymbol{Q}_1 \hat{\boldsymbol{e}}_{13}^T, \tag{42}$$
where $\boldsymbol{Q}_1$ is
$$\boldsymbol{Q}_1 \triangleq \begin{bmatrix} \sigma^3\Delta & -\dfrac{\mu\sigma^2\sqrt{h(e_2)}|X^{U_{rd}}|}{2\Delta} \\[2ex] -\dfrac{\mu\sigma^2\sqrt{h(e_2)}|X^{U_{rd}}|}{2\Delta} & \mu\eta h(e_2)\left(|Y^{U_{rd}}| - \dfrac{|X^{U_{rd}}|}{\Delta}\right) \end{bmatrix} \tag{43}$$
and $0 < \eta < 1$. L_2 is defined as
$$L_2 \triangleq \frac{\Delta}{h(e_2)} \hat{\boldsymbol{e}}_{23}^T \boldsymbol{Q}_2 \hat{\boldsymbol{e}}_{23}, \tag{44}$$
where $\boldsymbol{Q}_2$ is
$$\boldsymbol{Q}_2 \triangleq \begin{bmatrix} \beta & -\alpha\sqrt{h(e_2)} \\[1ex] -\alpha\sqrt{h(e_2)} & h(e_2)\dfrac{\alpha(2\alpha-1)}{\beta} \end{bmatrix}. \tag{45}$$
Here, $\beta \triangleq U_r - V_{\max} - \sigma$ and α is given by
$$\alpha \triangleq (1-\eta)\frac{(U_r - V_{\max} - \sigma)(\Delta|Y^{U_{rd}}| - |X^{U_{rd}}|)}{|X^{U_{rd}}|(U_r + V_{\max} + \sigma)}. \tag{46}$$
The parameter μ is chosen as
$$\mu \triangleq \frac{\Delta^2(2\alpha-1)}{|X^{U_{rd}}|(U_r + V_{\max} + \sigma)}. \tag{47}$$

If $\boldsymbol{Q}_1$ and $\boldsymbol{Q}_2$ are positive definite, then $\dot{W}$ is negative definite and the system (37) is uniformly stable. $\boldsymbol{Q}_1$ is positive definite if
$$\Delta > \frac{|X^{U_{rd}}|}{|Y^{U_{rd}}|}, \tag{48}$$
$$\mu < \frac{4\eta\Delta^2\left(\Delta|Y^{U_{rd}}| - |X^{U_{rd}}|\right)}{\sigma|X^{U_{rd}}|^2}. \tag{49}$$
(48) is met as long as (38) holds. It can be shown that $\eta \geq 1/5$ is a sufficient condition for μ to satisfy (49). Thus, without loss of generality, η is set to $1/5$, and positive definiteness of Q_1 is ensured.

$\boldsymbol{Q}_2$ is positive definite if $\beta > 0$ and $\alpha > 1$. Assumption 3 and (39) ensure that $\beta > 0$, while conditions (38) and (39) ensure that $\alpha > 1$. With positive definite $\boldsymbol{Q}_1$ and $\boldsymbol{Q}_2$ it follows that $\dot{W} < 0$. Since $W > 0$, (Khalil, 2002, Theorem 4.8) can be used to show that the equilibrium $\hat{\boldsymbol{e}} = \boldsymbol{0}$ is uniformly stable.

The Lyapunov function candidate W from (40) is split into
$$W = W_1(\hat{\boldsymbol{e}}_{13}) + W_2(\hat{\boldsymbol{e}}_{23}), \tag{50}$$
where
$$W_1 \triangleq \tfrac{1}{2}\hat{\boldsymbol{e}}_{13}^T P_1 \hat{\boldsymbol{e}}_{13}, \tag{51}$$
$$W_2 \triangleq \tfrac{1}{2}\hat{\boldsymbol{e}}_{23}^T P_2 \hat{\boldsymbol{e}}_{23}, \tag{52}$$
$P_1 = \text{diag}\left\{\sigma, \tfrac{1}{2}\mu\right\} > 0$ and $P_2 = \text{diag}\left\{1, \tfrac{1}{2}\mu\right\} > 0$. Hence, using (42) and (44),
$$\dot{W}_1 \leq \frac{-2}{h(e_2)}\frac{q_{1,\min}}{p_{1,\max}}W_1, \tag{53}$$
$$\dot{W}_2 \leq \frac{-2\Delta}{h(e_2)}\frac{q_{2,\min}}{p_{2,\max}}W_2. \tag{54}$$
where $q_{i,\min} = \lambda_{\min}(\boldsymbol{Q}_i)$, $p_{i,\max} = \lambda_{\max}(\boldsymbol{P}_i)$, $i \in \{1,2\}$. Applying the bound (26) on $h(e_2)$ in (53) and (54) leads to
$$\dot{W}_1 \leq -2c(r)\frac{q_{1,\min}}{p_{1\max}}W_1, \ \forall\|\hat{\boldsymbol{e}}(t)\| \leq r, \tag{55}$$
$$\dot{W}_2 \leq -2\Delta c(r)\frac{q_{2,\min}}{p_{2\max}}W_2, \ \forall\|\hat{\boldsymbol{e}}(t)\| \leq r. \tag{56}$$

Similarly to the derivation of (28), it is then possible to invoke the comparison lemma, which implies that for $w_1(t) = W_1(t, \hat{\boldsymbol{e}}(t))$ and $w_2(t) = W_2(t, \hat{\boldsymbol{e}}(t))$,
$$w_1 \leq e^{-2(q_{1,\min}/p_{1,\max})c(r)(t-t_0)}w_1(t_0), \tag{57}$$
$$w_2 \leq e^{-2(q_{2,\min}/p_{2,\max})\Delta c(r)(t-t_0)}w_2(t_0). \tag{58}$$
Consequently, for $w(t) = W(t, \hat{\boldsymbol{e}}(t))$,
$$w \leq e^{-2\rho c(r)(t-t_0)}w(t_0) \tag{59}$$
where $\rho = \min([q_{1,\min}/p_{1,\max}], [\Delta q_{2,\min}/p_{2,\max}])$. Therefore, with $p_{\max} \triangleq \max(\sigma^2, 1, \mu)$ and $p_{\min} \triangleq \min(\sigma^2, 1, \mu)$,
$$\|\hat{\boldsymbol{e}}(t)\| \leq \sqrt{\frac{p_{\max}}{p_{\min}}}e^{-\rho c(r)(t-t_0)}\|\hat{\boldsymbol{e}}(t_0)\| \tag{60}$$

Hence, the equilibrium point $\hat{\boldsymbol{e}} = \boldsymbol{0}$ is USGES as defined in (Loria and Panteley, 2004, Definition 2.7).

5.3 Stability property of the closed-loop system

Theorem 3. If Assumptions 1 to 3 hold and the look-ahead distance Δ and the integral gain σ satisfy
$$\Delta > \frac{|X^{U_{rd}}|}{|Y^{U_{rd}}|}\left[\frac{5}{4}\frac{U_{rd} + V_{\max} + \sigma}{U_{rd} - V_{\max} - \sigma} + 1\right], \tag{61}$$
$$0 < \sigma < U_r - V_{\max}, \tag{62}$$
then the controllers (9) and (10), where ψ_d is given by (8), guarantee achievement of the control objectives (7). Control objective (7b) is fulfilled with
$$\psi_{ss} = -\tan^{-1}(V_y/\sqrt{U_{rd}^2 - V_y^2}). \tag{63}$$
Furthermore, the equilibrium point of the error dynamics (33) is USGES and UGAS.

Proof. The system (33) is a cascaded system, consisting of a linear system (33b) which perturbs the dynamics (33a) through the interconnection matrix $\boldsymbol{H}$. The interconnection matrix $\boldsymbol{H}$ can be shown to satisfy $\|\boldsymbol{H}\| \leq \theta_1(\|\boldsymbol{\zeta}\|)(|y| + |y_{\mathrm{int}}| + |v_r|) + \theta_2(\|\boldsymbol{\zeta}\|)$, where $\theta_1(\cdot)$ and $\theta_2(\cdot)$ are some continuous non-negative functions.

The perturbing system (33b), described in detail in (29), is a linear, time-invariant system. Furthermore, since the gains k_{u_r}, k_ψ, k_r and the term d_{11}/m_{11} are all strictly positive, the system matrix $\boldsymbol{\Sigma}$ is Hurwitz and the origin $\boldsymbol{\zeta} = \boldsymbol{0}$ is UGES. Note, however, that any set of controllers providing USGES (or UGES) of the surge and yaw error dynamics will give the same result. This is due to the modular properties of the cascaded systems control theory that is used in the analysis.

The nominal system is USGES by Lemma 2. Hence all the conditions of (Loria and Panteley, 2004, Proposition 2.3) are satisfied, guaranteeing USGES and UGAS of the origin of (33).

Finally, ψ_{ss} can be shown to satisfy (63) by inserting the equilibrium values (31) into the ILOS control law (8a).

6. SIMULATIONS

This section presents results from numerical simulations of the ILOS guidance law applied to an underactuated AUV. The AUV is modeled in 3-DOF and tasked to follow a horizontal path along the x-axis. The desired relative surge speed is $U_{rd} = 2$ m/s. The current is set to $\boldsymbol{v}_c = [0.1\ \mathrm{m/s}, 0.3\ \mathrm{m/s}, 0\ \mathrm{rad/s}]$. The ocean current intensity is $\|\boldsymbol{v}_c\| = 0.3261$ m/s, which fulfills Assumption 1 and 3. It can be verified that Assumption 2 is satisfied with $Y_{\min} = 0.6509$ s^{-1}, and that (38) and (61) are satisfied with $|X^{U_{rd}}| = 0.1978$ and $|Y^{U_{rd}}| = 0.9096$. The ILOS look-ahead distance and integral gain are $\Delta = 10$ m and $\sigma = 0.2$ m/s, which satisfy (61)-(62). The surge and yaw controllers (9)-(10) are implemented with $k_{u_r} = 0.5$, $k_\psi = 1$ and $k_r = 2$. The initial position of the vehicle is 25m east of the path, the initial direction is parallel to the path and the initial velocity is zero.

In Figure 1 the position of the vessel in is shown, and the heading of the vessel is illustrated. Note that the vessel maintains a constant sideslip angle after converging to the path to counteract the current. Relative sway velocity v_r, and hence the drift angle with respect to the water flow, stabilizes at zero. Figure 2 shows how the cross-track error converges to zero. The cross-track error increases in the beginning, while the vessel is accelerating and turning to counter the current, and there is an overshoot due to the integral effect. Figure 3 shows the natural logarithm of the Euclidean norm of the error variables in (33), where $\hat{\boldsymbol{e}}_{\mathrm{tot}} \triangleq [\hat{\boldsymbol{e}}^T \boldsymbol{\zeta}^T]^T$. Notice that $\ln(\|\hat{\boldsymbol{e}}_{\mathrm{tot}}\|)$ is upper bounded by a straight, descending line, corresponding to a bounding exponential function of the form $\gamma_1 \mathrm{e}^{-\gamma_2(t-t_0)} \|\hat{\boldsymbol{e}}_{\mathrm{tot}}(t_0)\|$, for positive constants γ_1 and γ_2. Hence, for these initial conditions, exponential convergence of the system is verified.

The heading of the vessel can be difficult to measure in practice. Magnetic compasses, for example, are prone to errors due to disturbances in the surrounding magnetic field. Gyrocompasses, which estimate true north based on
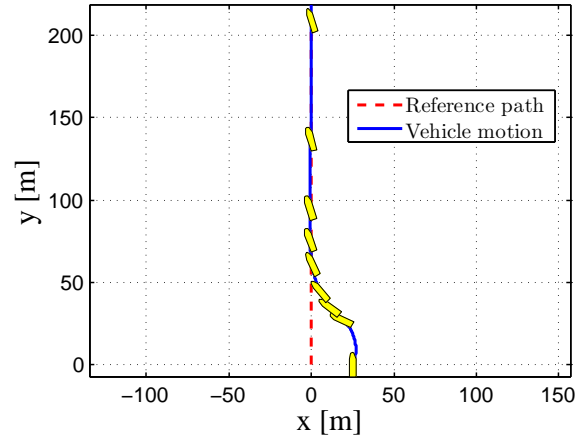

Fig. 1. Position and heading of the vehicle during the simulation. The time interval 0 - 180 s is considered in the figure.
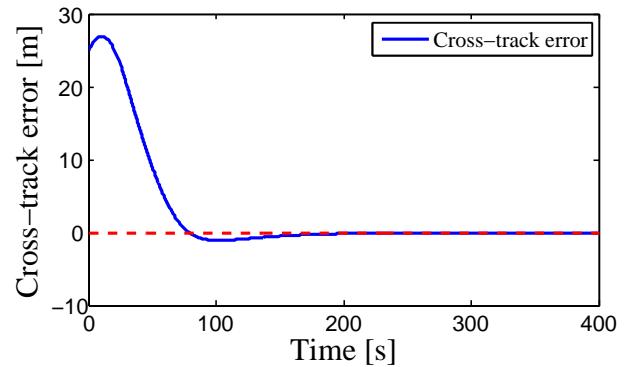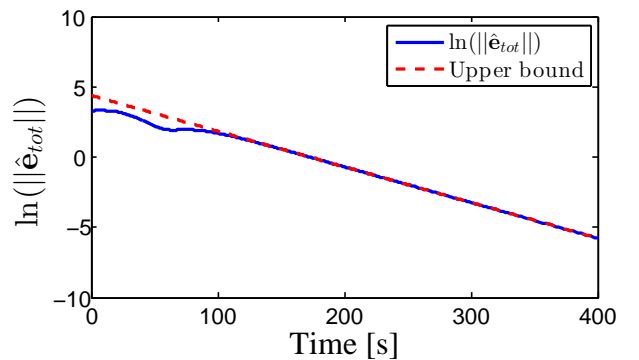

Fig. 2. The cross-track error y of the vessel.

Fig. 3. The natural logarithm of $\|\hat{\boldsymbol{e}}_{\mathrm{tot}}\|$.

the rotation of the earth, need long settling time when used in the high north. It is therefore of interest to investigate the performance of the guidance law in the presence of measurement errors in heading. While analysis of the robustness properties of the system has not been the aim of this paper, Figure 4 illustrates the performance of the system when simulated with a heading measurement error of 10 degrees. The vessel still converges to the path, even though the overshoot is larger and the convergence time slower.
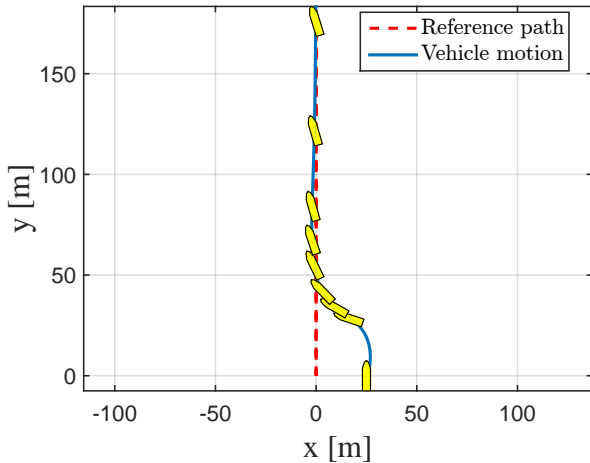
Fig. 4. Position and heading of the vehicle during the simulation with a heading measurement error of 10 degrees. The time interval 0 - 180 s is considered in the figure.

7. CONCLUSIONS

In this paper the stability properties of an underactuated marine vessel controlled by an ILOS guidance law has been investigated. The system has been proved to be USGES, which is a stronger stability property than κ-exponential stability which has been proven in the literature before. In addition, USGES guarantees stronger robustness properties of the system. The underactuated marine vessel has been modeled in 3-DOF, and the results are applicable both for surface vessels and for underwater vehicles moving in a horizontal plane. As an example of the latter, an AUV has been simulated in an ocean environment containing constant and irrotational currents, demonstrating exponential stability.

REFERENCES

Børhaug, E., Pavlov, A., and Pettersen, K.Y. (2008). Integral LOS control for path following of underactuated marine surface vessels in the presence of constant ocean currents. In *Proc. 47th IEEE Conference on Decision and Control*, 4984–4991. Cancun, Mexico.

Børhaug, E. and Pettersen, K.Y. (2005). Cross-track control for underactuated autonomous vehicles. In *Proc. 44th IEEE Conference on Decision and Control*, volume 2005, 602–608. Seville, Spain.

Breivik, M. and Fossen, T. (2004). Path following for marine surface vessels. In *Proc. Oceans '04 MTS/IEEE Techno-Ocean '04*, 2282–2289.

Breivik, M. and Fossen, T.I. (2009). Guidance laws for autonomous underwater vehicles. In A.V. Inzartsev (ed.), *Intelligent Underwater Vehicles*, chapter 4, 51–76. I-Tech Education and Publishing, Vienna, Austria.

Caharija, W., Pettersen, K.Y., Sørensen, A.J., Candeloro, M., and Gravdahl, J.T. (2014). Relative velocity control and integral line of sight for path following of autonomous surface vessels: Merging intuition with theory. In *Proc. Institution of Mechanical Engineers, Part M: Journal of Engineering for the Maritime Environment*, volume 228, 180–191.

Caharija, W., Candeloro, M., Pettersen, K.Y., and Sørensen, A.J. (2012a). Relative velocity control and integral LOS for path following of underactuated surface vessels. In *Proc. 9th IFAC Conference on Manuevering and Control of Marine Craft*, volume 9, 380–385.

Caharija, W., Pettersen, K.Y., and Gravdahl, J.T. (2013). Path following of underactuated surface vessels in presence of unknown constant environmental forces: Preliminary results. In *Proc. 9th IFAC Conference on Control Applications in Marine Systems*, 85–90. Osaka, Japan.

Caharija, W., Pettersen, K.Y., Bibuli, M., Calado, P., Zereik, E., Braga, J., Gravdahl, J.T., Sørensen, A.J., Milovanović, M., and Bruzzone, G. (2015). Integral line-of-sight guidance and control of underactuated marine vehicles. Submitted to *IEEE Transactions on Control Systems Technology*. Available at https://www.dropbox.com/sh/p0u29befp1gwwjr/AABvgwo_lqC7252E516t_b_Xa.

Caharija, W., Pettersen, K.Y., Gravdahl, J.T., and Børhaug, E. (2012b). Path following of underactuated autonomous underwater vehicles in the presence of ocean currents. In *Proc. 51st IEEE Conference on Decision and Control*, 528–535. Maui, HI.

Dubins, L.E. (1957). On curves of minimal length with a constraint on average curvature, and with prescribed initial and terminal positions and tangents. *American Journal of mathematics*, 79(3), 497–516.

Encarnação, P. and Pascoal, A. (2001). Combined trajectory tracking and path following: An application to the coordinated control of autonomous marine craft. In *Proc. 40th IEEE Conference on Decision and Control*, December, 964–969. Orlando,FL.

Fossen, T.I. (2011). *Handbook of marine craft hydrodynamics and motion control*. John Wiley & Sons.

Fossen, T.I. and Pettersen, K.Y. (2014). On uniform semiglobal exponential stability (USGES) of proportional line-of-sight guidance laws. *Automatica*, 50(11), 2912–2917.

Fossen, T.I., Pettersen, K.Y., and Galeazzi, R. (2014). Line-of-sight path following for Dubins paths with adaptive sideslip compensation of drift forces. *IEEE Transactions on Control Systems Technology*, 23(2), 820–827.

Fossen, T., Breivik, M., and Skjetne, R. (2003). Line-of-sight path following of underactuated marine craft. In *Proc. 6th IFAC Conference on Manoeuvring and Control of Marine Craft*, 244–249. Girona, Spain.

Fredriksen, E. and Pettersen, K. (2006). Global κ-exponential way-point maneuvering of ships: Theory and experiments. *Automatica*, 42(4), 677–687.

Healey, A. and Lienard, D. (1993). Multivariable sliding mode control for autonomous diving and steering of unmanned underwater vehicles. *Oceanic Engineering, IEEE Journal of*, 18(3), 327–339.

Khalil, H.K. (2002). *Nonlinear Systems*. Pearson Education International inc., 3rd edition.

Lekkas, A.M. and Fossen, T.I. (2014). Integral LOS path following for curved paths based on a monotone cubic Hermite spline parametrization. *IEEE Transactions on Control Systems Technology*, 22(6), 2287–2301.

Loria, A. and Panteley, E. (2004). Cascaded nonlinear time-varying systems: analysis and design. In F. Lamnabhi-Lagarrigue, A. Loria, and E. Panteley (eds.), *Advanced Topics in Control Systems Theory*,

chapter 2, 23–64. Springer Verlag, London.

Pettersen, K. and Lefeber, E. (2001). Way-point tracking control of ships. In *Proc. 40th IEEE Conference on Decision and Control*, 940–945. Orlando, FL.

Sørdalen, O.J. and Egeland, O. (1995). Exponential stabilization of nonholonomic chained systems. *IEEE Transactions on Automatic Control*, 40(1), 35–49.

Appendix A. FUNCTIONAL EXPRESSIONS

$$F_{u_r}(v_r, r) \triangleq \frac{1}{m_{11}}(m_{22}v_r + m_{23}r)r \tag{A.1}$$

$$X(u_r) \triangleq \frac{m_{23}^2 - m_{11}m_{33}}{m_{22}m_{33} - m_{23}^2}u_r + \frac{d_{33}m_{23} - d_{23}m_{33}}{m_{22}m_{33} - m_{23}^2} \tag{A.2}$$

$$Y(u_r) \triangleq \frac{(m_{22} - m_{11})m_{23}}{m_{22}m_{33} - m_{23}^2}u_r - \frac{d_{22}m_{33} - d_{32}m_{23}}{m_{22}m_{33} - m_{23}^2} \tag{A.3}$$

$$F_r(u_r, v_r, r) \triangleq \frac{m_{23}d_{22} - m_{22}(d_{32} + (m_{22} - m_{11}u_r)}{m_{22}m_{33} - m_{23}^2}v_r$$
$$+ \frac{m_{23}(d_{23} - m_{11}u_r) - m_{22}(d_{33} + m_{23}u_r}{m_{22}m_{33} - m_{23}^2}$$

The functions $\boldsymbol{h}_{e_2} \triangleq [h_{e_21}, h_{e_22}, h_{e_23}]^T$ is defined as

$$h_{e_21} = \sin(\tilde{\psi} + \psi_d), \quad h_{e_23} = 0,$$

$$h_{e_22} = U_{rd}\left[\frac{\sin(\tilde{\psi})}{\tilde{\psi}}\cos(\psi_d) + \frac{\cos(\tilde{\psi}) - 1}{\tilde{\psi}}\sin(\psi_d)\right]$$
$$+ e_3\left[\frac{\cos(\tilde{\psi}) - 1}{\tilde{\psi}}\cos(\psi_d) - \frac{\sin(\tilde{\psi})}{\tilde{\psi}}\sin(\psi_d)\right], \tag{A.4}$$

and $\boldsymbol{h}_{e_3} \triangleq [h_{e_31}, h_{e_32}, h_{e_33}]^T$ is

$$h_{e_31} = \frac{X(\tilde{u}_r + U_{rd}) - X^{U_{rd}}}{\tilde{u}_r}\gamma(e_2, e_3)$$
$$+ e_3\frac{Y(\tilde{u}_r + U_{rd}) - Y^{U_{rd}}}{\tilde{u}_r}, \tag{A.5}$$
$$h_{e_32} = 0, \quad h_{e_33} = X(\tilde{u}_r + U_{rd}).$$

The limits of h_{e_22} for $\tilde{\psi} \to 0$ and h_{e_31} as $\tilde{u}_r \to 0$ exist and are finite. The expression $\rho(e_2, e_3)$ used in h_{e_31} is defined as

$$\gamma(e_2, e_3) \triangleq \frac{\Delta U_{rd}(e_2 + \sigma y_{\text{int}}^{\text{eq}}) - \Delta^2 e_3}{h(e_2)^{3/2}}$$
$$- \frac{\sigma\Delta^2}{h(e_2)^2}y - \frac{\Delta V_y}{h(e_2)} \tag{A.6}$$